

# Development of High-Order Realizable Finite-Volume Schemes for Quadrature-Based Moment Method

V. Vikas<sup>1</sup> and Z. J. Wang<sup>2</sup>

*Department of Aerospace Engineering, Iowa State University, Ames, IA, 50011*

A. Passalacqua<sup>3</sup> and R. O. Fox<sup>4</sup>

*Department of Chemical and Biological Engineering, Iowa State University, Ames, IA, 50011*

**Kinetic equations containing terms for spatial transport, gravity, fluid drag and particle-particle collisions can be used to model dilute gas-particle flows. However, the enormity of independent variables makes direct numerical simulation of these equations almost impossible for practical problems. A viable alternative is to reformulate the problem in terms of moments of velocity distribution. Recently, a quadrature-based moment method was derived by Fox for approximating solutions to kinetic equation for arbitrary Knudsen number. Fox also described 1<sup>st</sup>- and 2<sup>nd</sup>-order finite-volume schemes for solving the equations. The success of the new method is based on a moment-inversion algorithm that is used to calculate non-negative weights and abscissas from moments. The moment-inversion algorithm does not work if the moments are non-realizable, meaning they do not correspond to a distribution function. Not all the finite-volume schemes lead to realizable moments. Desjardins et al. showed that realizability is guaranteed with the 1<sup>st</sup>-order finite-volume scheme, but at the expense of excess numerical diffusion. In the present work, the non-realizability of the standard 2<sup>nd</sup>-order finite-volume scheme is demonstrated and a generalized idea for the development of high-order realizable finite-volume schemes for quadrature-based moment methods is presented. This marks a significant improvement in the accuracy of solutions using the quadrature-based moment method as the use of 1<sup>st</sup>-order scheme to guarantee realizability is no longer a limitation.**

## I. Introduction

**G**AS-PARTICLE flows are ubiquitous in aerospace, mechanical, chemical and many other engineering disciplines. One finds such flows in automotive and aircraft engines, snow and sand storms, helicopter brownout phenomenon, and many other critical situations. The understanding of the flow characteristics is crucial in improving the performance of gas-turbine engines, or mitigating the harmful effects of helicopter brownout.

The numerical simulation of gas-particle flows is complicated by the wide range of phenomena that can occur in real applications [1, 2, 3, 4, 5, 6, 7, 8, 9]. In the case of helicopter brownout, the number of particles is so large that it is impossible to track the motion of each one. In addition, these particles may have very different sizes and shapes. It is well known that the traditional multiphase flow solvers based on the volume-of-fluid (VOF) method [15, 16, 17] or the level-set method [18, 19, 20, 21] are hopeless for such applications, and Lagrangian particle tracking methods [22, 23, 24] are also very inefficient. In many other applications, physical complexities may include particle breaking, merging (or coalescence), and evaporation [25]. It appears, the only method that can handle these physical complexities is a kinetic-based method that solves for the moments of the velocity distribution function.

Fox [5, 10, 11, 12, 13] developed a quadrature-based moment method (QMOM) to solve for a set of moments of the velocity distribution function. The success of this method is based on a moment-inversion algorithm that is used to calculate non-negative weights and abscissas from moments. The moment-inversion algorithm does not work if

---

<sup>1</sup> Graduate Research Assistant, Department of Aerospace Engineering, 2271 Howe Hall, AIAA Member.

<sup>2</sup> Professor of Aerospace Engineering, 2271 Howe Hall, Associate Fellow of AIAA.

<sup>3</sup> Postdoctoral Research Fellow, Department of Chemical and Biological Engineering, 2114 Sweeney Hall

<sup>4</sup> Professor of Chemical and Biological Engineering, 2114 Sweeney Hall.

the moments are non-realizable. Not all the finite-volume schemes lead to realizable moments. Desjardins et al. [1] showed that realizability is guaranteed with 1<sup>st</sup>-order finite-volume scheme that has high inherent numerical diffusion. In the present work, the non-realizability of the standard 2<sup>nd</sup>-order finite-volume scheme is demonstrated and a generalized idea for the development of high-order realizable finite-volume schemes for quadrature-based moment methods is presented.

The paper is organized as follows. In Section 2, QMOM is reviewed and realizability of 1<sup>st</sup>-order finite-volume scheme is revisited. The non-realizability of standard 2<sup>nd</sup>-order finite-volume scheme is also discussed in Section 2. Thereafter, in Section 3, new realizable high-order finite-volume schemes are presented. Section 4 presents some numerical results including accuracy studies. Conclusions for the present study are summarized in Section 5.

## II. Quadrature Method Of Moments (QMOM)

### 2.1 Kinetic Theory of Dilute Particle Flows

Dilute gas-particle flows can be modeled by a kinetic equation [26, 27, 28] of the form

$$\partial_t f + \mathbf{v} \cdot \partial_x f + \partial_v \cdot (f \mathbf{F}) = \mathbb{C} \quad (2.1)$$

where  $f(\mathbf{v}, \mathbf{x}, t)$  is the velocity based number density function,  $\mathbf{v}$  is the particle velocity,  $\mathbf{F}$  is the force acting on individual particle, and  $\mathbb{C}$  is the collision term, representing the rate of change in the velocity distribution function due to collisions. The collision term can be described using Bhatnagar-Gross-Krook (BGK) collision operator [29]:

$$\mathbb{C} = \frac{1}{\tau} (f_{eq} - f) \quad (2.2)$$

where  $\tau$  is the characteristic collision time, and  $f_{eq}$  is the Maxwellian equilibrium velocity distribution,

$$f_{eq}(\mathbf{v}) = \frac{M^0}{\sqrt{(2\pi\sigma_{eq})^3}} \exp\left(-\frac{|\mathbf{v} - \mathbf{U}_p|^2}{2\sigma_{eq}}\right) \quad (2.3)$$

in which  $\mathbf{U}_p$  is the mean particle velocity,  $\sigma_{eq}$  is the equilibrium variance and  $M^0$  is the particle number density. In gas-particle flows, the force term is given by the sum of the gravitational contribution and the drag term exerted from the fluid on the particles:

$$\mathbf{F} = \mathbf{F}_g + \mathbf{F}_d \quad (2.4)$$

For dilute gas-particle flows, the drag force on a particle can be approximated by

$$\mathbf{F}_d = \frac{3m_p\rho_g}{4\rho_p d_p} C_d |\mathbf{U}_r| \mathbf{U}_r \quad (2.5)$$

where  $\mathbf{U}_r = \mathbf{U}_g - \mathbf{U}_p$  is the relative velocity between two phases,  $\mathbf{U}_g$  is the gas velocity,  $\mathbf{U}_p$  is the particle phase local mean velocity,  $\rho_g$  and  $\rho_p$  are gas and particle densities and  $d_p$  the particle diameter. The drag coefficient  $C_d$  is given by Schiller & Nauman correlation [30].

$$C_d = \frac{24}{Re_p} (1 + 0.15 Re_p^{0.687}) \quad (2.6)$$

in which  $Re_p = \rho_g d_p |\mathbf{U}_g - \mathbf{U}_p| / \mu_g$ ,  $\mu_g$  being the dynamic viscosity of gas phase.

### 2.2 Moment transport equations

In the quadrature-based moment methods (QMOM) of Fox [5, 13], a set of moments of number density function  $f$  are transported and their evolution in space and time is tracked. Each element of the moment set is defined through integrals of the velocity distribution function as

$$\begin{aligned} M^0 &= \int f d\mathbf{v} & M_i^1 &= \int v_i f d\mathbf{v} \\ M_{ij}^2 &= \int v_i v_j f d\mathbf{v} & M_{ijk}^3 &= \int v_i v_j v_k f d\mathbf{v} \end{aligned} \quad (2.7)$$

where the superscript of  $M$  represents the order of corresponding moment. Moment transport equations are obtained by applying the definition of moments to (2.7), leading to the following set of partial differential equations in moments:

$$\begin{aligned} \frac{\partial M^0}{\partial t} + \frac{\partial M_i^1}{\partial x_i} &= 0 \\ \frac{\partial M_i^1}{\partial t} + \frac{\partial M_{ij}^2}{\partial x_j} &= g_i M^0 + D_i^1 \\ \frac{\partial M_{ij}^2}{\partial t} + \frac{\partial M_{ijk}^3}{\partial x_k} &= g_i M_j^1 + g_j M_i^1 + C_{ij}^2 + D_{ij}^2 \end{aligned} \quad (2.8)$$

$$\frac{\partial M_{ijk}^3}{\partial t} + \frac{\partial M_{ijkl}^4}{\partial x_l} = g_i M_{jk}^2 + g_j M_{ik}^2 + g_k M_{ij}^2 + C_{ijk}^3 + D_{ijk}^3$$

where  $D_i^1$ ,  $D_{ij}^2$  and  $D_{ijk}^3$  are due to the drag force and the terms containing  $g_i$ ,  $g_j$  and  $g_k$  are due to gravity.

### 2.3 Quadrature-based closures

The set of transport equations for the moments reported in (2.8) is unclosed because each equation contains the spatial fluxes of the moments of order immediately higher, and the collision and drag source terms. In quadrature-based moment methods quadrature formula are used to provide closures to the source terms in the moment transport equations, by introducing a set of  $\beta$  weights  $n_\alpha$  and abscissas  $\mathbf{U}_\alpha$ , which are determined from the moments of the distribution function using an inversion algorithm. The inversion algorithm is explained in detail in Fox [5].

The distribution function  $f$  is written in terms of the quadrature weights and abscissas using Dirac delta representation.

$$f(\mathbf{v}) = \sum_{\alpha=1}^{\beta} n_\alpha \delta(\mathbf{v} - \mathbf{U}_\alpha) \quad (2.9)$$

The moments can be computed as a function of quadrature weights and abscissas by approximating the integrals in (2.7) with summations:

$$\begin{aligned} M^0 &= \sum_{\alpha=1}^{\beta} n_\alpha & M_i^1 &= \sum_{\alpha=1}^{\beta} n_\alpha U_{\alpha i} \\ M_{ij}^2 &= \sum_{\alpha=1}^{\beta} n_\alpha U_{\alpha i} U_{\alpha j} & M_{ijk}^3 &= \sum_{\alpha=1}^{\beta} n_\alpha U_{\alpha i} U_{\alpha j} U_{\alpha k} \end{aligned} \quad (2.10)$$

The source terms due to drag and gravity are computed as

$$\begin{aligned} D_i^1 &= \sum_{\alpha=1}^{\beta} n_\alpha \left( \frac{F_{i\alpha}}{m_p} - \delta_{i2} g \right) \\ D_{ij}^2 &= \sum_{\alpha=1}^{\beta} n_\alpha \left[ \left( \frac{F_{i\alpha}}{m_p} - \delta_{i2} g \right) U_{j\alpha} + \left( \frac{F_{j\alpha}}{m_p} - \delta_{j2} g \right) U_{i\alpha} \right] \\ D_{ijk}^3 &= \sum_{\alpha=1}^{\beta} n_\alpha \left[ \left( \frac{F_{i\alpha}}{m_p} - \delta_{i2} g \right) U_{j\alpha} U_{k\alpha} + \left( \frac{F_{j\alpha}}{m_p} - \delta_{j2} g \right) U_{k\alpha} U_{i\alpha} + \left( \frac{F_{k\alpha}}{m_p} - \delta_{k2} g \right) U_{i\alpha} U_{j\alpha} \right] \end{aligned} \quad (2.11)$$

The details of computation of drag force terms,  $F_{i\alpha}$ ,  $F_{j\alpha}$  and  $F_{k\alpha}$ , can be found in [5]. The spatial flux terms are closed according to their kinetic description [1, 31]. Each moment involved in the spatial derivative is decomposed in two contributions, as shown in (2.12) for the first-order moments.

$$M_i^1 = \int_{-\infty}^0 v_i (f dv_j dv_k) dv_i + \int_0^{+\infty} v_i (f dv_j dv_k) dv_i \quad (2.12)$$

Using (2.9), (2.12) can be written as:

$$M_i^1 = \sum_{\alpha=1}^{\beta} n_\alpha \min(0, U_{i\alpha}) + \sum_{\alpha=1}^{\beta} n_\alpha \max(0, U_{i\alpha}) \quad (2.13)$$

For collisions, the source terms in the moment transport equations are given by:

$$\begin{aligned} C_{ij}^2 &= \frac{M^0}{\tau} (\sigma_{eq} \delta_{ij} - \sigma_{ij}) \\ C_{ijk}^3 &= \frac{1}{\tau_c} (\Delta_{ijk} - M_{ijk}^3) \end{aligned} \quad (2.14)$$

where  $\sigma_{eq}$ ,  $\tau_c$  and  $\Delta_{ijk}$  are respectively the variance, collision time and the set of third-order moments of the equilibrium distribution function.

### 2.4 Boundary conditions

Although, it is equally valid to write the boundary conditions for the moment transport equations in terms of the moments, it is more convenient to write them in terms of weights and abscissas. In this work three types of boundary conditions are used – fix-all, periodic and wall-reflective. At fix-all boundary, the weights and abscissas are specified. Periodic boundary conditions copy the weights and abscissas from the outgoing periodic boundary cell to the corresponding incoming periodic boundary cell. The boundary conditions at the walls are set so that particle that collides with the wall is specularly reflected. This condition corresponds to changing the sign of the velocity component of the particle along the direction perpendicular to the wall. The implementation of this boundary condition in the quadrature-based algorithm is done by changing the sign of the abscissas in the appropriate direction [5]. If  $i=0$  indicates the position of the wall, perpendicular to the second direction of reference frame, and  $i=1$  indicates the neighboring computational cell, the boundary condition can be written as

$$\begin{pmatrix} n_\alpha \\ U_\alpha \\ V_\alpha \\ W_\alpha \end{pmatrix}_{i=0} = \begin{pmatrix} n_\alpha/e_w \\ U_\alpha \\ -e_w V_\alpha \\ W_\alpha \end{pmatrix}_{i=1} \quad (2.15)$$

where  $e_w$  is the paricle-wall restitution coefficient.

### 2.5 Non-realizability problem

The moment-inversion algorithm computes the set of weights and abscissas from the corresponding set of moments by solving a set of nonlinear equations. To discuss the problem of realizability, a simplified one-dimensional case with 2 quadrature nodes is considered here. For this case, the set of moment equations after dropping collision and drag terms can be written as

$$\frac{\partial W}{\partial t} + \frac{\partial H(W)}{\partial x} = 0 \quad (2.16a)$$

where,

$$W = [M^0 \ M^1 \ M^2 \ M^3] \quad \text{and} \quad H(W) = [M^1 \ M^2 \ M^3 \ M^4] \quad (2.16b)$$

If the set of weights and abscissas for 2-node quadrature case are  $(n_1, U_1)$  and  $(n_2, U_2)$ , the first four moments can be written as:

$$\begin{aligned} M^0 &= n_1(U_1)^0 + n_2(U_2)^0 \\ M^1 &= n_1(U_1)^1 + n_2(U_2)^1 \\ M^2 &= n_1(U_1)^2 + n_2(U_2)^2 \\ M^3 &= n_1(U_1)^3 + n_2(U_2)^3 \end{aligned} \quad (2.17)$$

In the equations for  $M^0$  and  $M^1$ , powers of  $U_1$  and  $U_2$  are redundant. In moment inversion algorithm  $M^0, M^1, M^2, M^3$  are known and  $n_1, n_2, U_1, U_2$  are computed, by solving the above set of equations in reverse direction. However, any arbitrary set of weights and abscissas do not conform to the definition of  $f$  in (2.9). Only the set of weights and abscissas that are realizable are allowed. A set of weights and abscissas or the set of moments from which it is computed is called realizable, if the weights are non-negative and abscissas lie in the interior of the support of  $f$ . Because of the non-linearity of inversion problem, it is extremely difficult to determine in advance whether a given set of moments is realizable. However, Desjardins et al. [1] described that any finite-volume scheme that could guarantee positivity of the effective velocity distribution function (explained below) will always keep the moments in realizable space.

The conservative moments and moment fluxes in (2.16a) can be written in terms of velocity distribution function.

$$\begin{aligned} W &= \int K(v) f_w(v) dv \\ H(W) &= \int v K(v) f_w(v) dv \end{aligned} \quad (2.18a)$$

where

$$K(v) = [1 \ v \ v^2 \ v^3] \quad (2.18b)$$

However, when a finite-volume scheme is used to advance the conservative moments in time, the form of the updated moments differs from the one given in (2.18a). Assuming that the moments at time level  $n$  are realizable, the moments at time level  $(n+1)$  for  $i^{th}$  cell can be written as

$$W_i^{n+1} = W_i^n - \frac{\Delta t}{\Delta x} \left( G(W_{(i+1/2)}^n|_l, W_{i+1/2}^n|_r) - G(W_{i-1/2}^n|_l, W_{i-1/2}^n|_r) \right) \quad (2.19)$$

where  $G$  is the numerical flux function evaluated at cell interfaces, and  $l$  and  $r$  denote the left and right states at the interfaces respectively.  $G$  is defined as

$$G(W_l, W_r) = \int \frac{1}{2} (v + |v|) K(v) f_{W_l}(v) dv + \int \frac{1}{2} (v - |v|) K(v) f_{W_r}(v) dv \quad (2.20a)$$

or

$$G(W_l, W_r) = \int v^{+ve} K(v) f_{W_l}(v) dv + \int v^{-ve} K(v) f_{W_r}(v) dv \quad (2.20b)$$

This corresponds to a splitting between particles going from left to right (first term) and particles going from right to left (second term). Inserting the expression for  $f_w$  (2.9) yields

$$G(W_l, W_r) = H^+(W_l) + H^-(W_r) \quad (2.21a)$$

with

$$\begin{aligned}
H^+(W_l) &= n_{1l} \max(U_{1l}, 0) \begin{pmatrix} 1 \\ U_{1l} \\ U_{1l}^2 \\ U_{1l}^3 \end{pmatrix} + n_{2l} \max(U_{2l}, 0) \begin{pmatrix} 1 \\ U_{2l} \\ U_{2l}^2 \\ U_{2l}^3 \end{pmatrix} \\
H^-(W_r) &= n_{1r} \min(U_{1r}, 0) \begin{pmatrix} 1 \\ U_{1r} \\ U_{1r}^2 \\ U_{1r}^3 \end{pmatrix} + n_{2r} \min(U_{2r}, 0) \begin{pmatrix} 1 \\ U_{2r} \\ U_{2r}^2 \\ U_{2r}^3 \end{pmatrix}
\end{aligned} \tag{2.21b}$$

The updated set of moments can be written as:

$$W_i^{n+1} = \int K(v)g(v)dv \tag{2.22a}$$

where

$$g(v) = f_{W_i^n} - \lambda \left( v^{+ve} f_{W_{(i+1/2)l}^n}(v) + v^{-ve} f_{W_{(i+1/2)r}^n}(v) - v^{+ve} f_{W_{(i-1/2)l}^n}(v) - v^{-ve} f_{W_{(i-1/2)r}^n}(v) \right) \tag{2.22b}$$

Using (2.9),  $g(v)$  can be written in terms of weights and abscissas:

$$\begin{aligned}
g(v) &= \sum_{\alpha=1}^2 [n_{i\alpha}^n \delta(v - U_{i\alpha}^n) \\
&\quad - \lambda \{ v^{+ve} n_{(i+1/2)\alpha l}^n \delta(v - U_{(i+1/2)\alpha l}^n) + v^{-ve} n_{(i+1/2)\alpha r}^n \delta(v - U_{(i+1/2)\alpha r}^n) \\
&\quad - v^{+ve} n_{(i-1/2)\alpha l}^n \delta(v - U_{(i-1/2)\alpha l}^n) - v^{-ve} n_{(i-1/2)\alpha r}^n \delta(v - U_{(i-1/2)\alpha r}^n) \}]
\end{aligned} \tag{2.22c}$$

In (2.22),  $g(v)$  is an effective velocity distribution function and has different forms for different finite-volume schemes. Desjardins et al. [1] stated that any finite-volume scheme that guarantees positivity of  $g(v)$ , is realizable. Using this proposition, Desjardins et al. derived the realizability criterion for 1<sup>st</sup>-order finite-volume scheme. In the next section, the realizability criterion for 1<sup>st</sup>-order finite-volume scheme is revisited and the non-realizability problem with standard 2<sup>nd</sup>-order finite-volume scheme is discussed. For simplicity, the 1D version of schemes is discussed.

However, before the discussion on realizability or non-realizability of finite-volume schemes, certain important things must be stated. A non-realizable finite-volume scheme may not be non-realizable for all the problems. When a finite-volume scheme is said to be non-realizable, it just means that realizability for that scheme cannot be guaranteed for any general problem. However, there may still exist some problems for which a non-realizable scheme will always give a perfectly realizable set of moments. But, when a non-realizable scheme is used and the non-realizability problem occurs at even one time level, the weights and abscissas are computed wrongly at that time level and the final numerical solution may be completely unphysical. Therefore, it is strongly advised to use realizable finite-volume schemes with models based on quadrature-based moment methods.

### 2.5.1 First-order finite-volume scheme

The 1<sup>st</sup>-order finite-volume scheme for solving moment equations uses a piecewise constant approximation and is described in [1]. The weights and abscissas are assumed to be constant over a cell. For the 1<sup>st</sup>-order scheme, the interface terms in (2.19) can be written as:

$$W_{i+1/2}^n|_l = W_i^n \quad W_{i+1/2}^n|_r = W_{i+1}^n \quad W_{i-1/2}^n|_l = W_{i-1}^n \quad W_{i-1/2}^n|_r = W_i^n \tag{2.23}$$

As shown in [1], the effective velocity distribution function for 1<sup>st</sup> order finite volume scheme can be written as

$$g(v) = (1 - \lambda|v|)f_{W_i^n}(v) + \lambda v^+ f_{W_{i-1}^n}(v) - \lambda v^- f_{W_{i+1}^n}(v) \tag{2.24}$$

where  $\lambda = \Delta t / \Delta x$ . As the moments at time level  $n$  are assumed to be realizable, the positivity of velocity distribution function at time level  $n$  is guaranteed, i.e.  $f_{W_i^n}(v) > 0$ ,  $f_{W_{i-1}^n}(v) > 0$  and  $f_{W_{i+1}^n}(v) > 0$ . Also,  $v^+$  is always positive and  $v^-$  is always negative. Hence, the positivity of  $g(v)$  will be guaranteed if  $(1 - \lambda|v|) > 0$ . When written in terms of abscissas, this condition becomes

$$\lambda < \frac{1}{\max(|U_{1i}^n|, |U_{2i}^n|)} \tag{2.25}$$

Desjardins et al. derived this condition in [1].

### 2.5.2 Second-order finite-volume scheme

In 2<sup>nd</sup>-order finite-volume scheme, the MUSCL technique [32, 33, 36, 37] is used to obtain a piecewise linear reconstruction for weights and abscissas. The interface terms in (2.19) are constructed by

$$\begin{aligned}
W_{i-1/2}^n|_l &= W_{i-1}^n + \frac{1}{2}\phi(\rho_{i-1})(W_i^n - W_{i-1}^n) \\
W_{i-1/2}^n|_r &= W_i^n - \frac{1}{2}\phi(\rho_i)(W_{i+1}^n - W_i^n) \\
W_{i+1/2}^n|_l &= W_i^n + \frac{1}{2}\phi(\rho_i)(W_{i+1}^n - W_i^n) \\
W_{i+1/2}^n|_r &= W_{i+1}^n - \frac{1}{2}\phi(\rho_{i+1})(W_{i+2}^n - W_{i+1}^n)
\end{aligned} \tag{2.26a}$$

where  $\phi$  is a limiter and the ratio  $\rho$  is defined by

$$\rho_i = \frac{W_i^n - W_{i-1}^n}{W_{i+1}^n - W_i^n} \tag{2.26b}$$

Reconstruction without a limiter can introduce numerical oscillations by creating new local extrema. For the numerical results presented in this paper, the min-mod limiter [37] is used. The min-mod limiter can be written as:

$$\phi(\rho) = \max[0, \min(1, \rho)] \quad \text{with} \quad \lim_{\rho \rightarrow \infty} \phi(\rho) = 1 \tag{2.27}$$

The effective velocity distribution function for 2<sup>nd</sup>-order finite-volume scheme can be obtained from (2.22c), by filling in appropriate values for weights and abscissas reconstructed at interfaces. However, in order to show that the standard 2<sup>nd</sup>-order finite-volume scheme does not guarantee realizability, such an operation is not needed. On the right hand side of (2.22b), there are three positive terms (first, third and fourth) and two negative terms (second and fifth). For no particular value of  $\lambda$ , the positivity of  $g(v)$  can be guaranteed. Thus according to the proposition given in [1], standard 2<sup>nd</sup>-order finite-volume scheme is not always realizable and the moments may go out of realizable space. If this happens, weights and abscissas cannot be computed accurately.

## 2.6 Solution algorithm

The specification of the source terms, the spatial fluxes and the boundary conditions provides a closed set of partial differential equations. A detailed solution algorithm for these partial differential equations can be found in [13]. Here a brief overview of the steps involved in the solution procedure is presented, assuming a single stage Euler explicit time integration.

- a) Initialize weights and abscissas in the domain
- b) Compute moments using weights and abscissas
- c) Compute time step size  $\Delta t$
- d) Reconstruct weights and abscissas at cell faces
- e) Compute spatial flux terms at cell faces
- f) Advance moments by  $\Delta t$  due to spatial flux terms using a finite-volume approach
- g) Compute weights and abscissas from moments using moment-inversion algorithm
- h) Advance weights by  $\Delta t$  due to body force terms (drag and gravity)
- i) Compute moments using weights and abscissas
- j) Advance moments by  $\Delta t$  due to collision terms
- k) Compute weights and abscissas from moments using moment-inversion algorithm
- l) Apply boundary conditions to weights and abscissas
- m) Repeat steps (c) through (l) at each time step.

## III. New realizable finite-volume schemes

In general, all the terms of (2.22b) will not always sum up to a non-negative number. This is because some of the coefficients of  $f$  are negative. However, the coefficients of all the terms are not of the same order of magnitude. By setting  $\lambda$  to a value less than 1, the coefficient of the first term can be made larger than the coefficients of the other four terms. Taking this fact into consideration, if somehow the two negative terms (second and fifth) in (2.22b) can be grouped together with the first term, adjusting  $\lambda$  to a proper value could be helpful in guaranteeing the positivity of effective velocity distribution function. More specifically, (2.22b) can be written as:

$$g(v) = f_{W_i^n} - \lambda v^{+ve} f_{W_{(i+1/2)l}^n}(v) + \lambda v^{-ve} f_{W_{(i-1/2)r}^n}(v) + \text{positive terms} \tag{3.1}$$

One such grouping can be done in the 1<sup>st</sup>-order finite-volume scheme because,  $W_i^n = W_{(i+1/2)l}^n = W_{(i-1/2)r}^n$ , which implies  $f_{W_i^n} = f_{W_{(i+1/2)l}^n} = f_{W_{(i-1/2)r}^n}$ . As in the standard 2<sup>nd</sup>-order finite-volume scheme, the cell averaged moment is not equal to reconstructed moments in cell  $i$ , any such grouping of terms is not possible. However, a similar grouping of terms is still possible under some constraints. (3.1) in terms of weights and abscissas can be written as:

$$g(v) = \sum_{\alpha=1}^2 [n_{i\alpha}^n \delta(v - U_{i\alpha}^n) - \lambda v^{+ve} n_{(i+1/2)al}^n \delta(v - U_{(i+1/2)al}^n) + \lambda v^{-ve} n_{(i-1/2)ar}^n \delta(v - U_{(i-1/2)ar}^n)] \quad (3.2)$$

+ *positive terms*

For any general reconstruction, other than 1<sup>st</sup>-order,  $n_{i\alpha}^n \neq n_{(i+1/2)al}^n \neq n_{(i-1/2)ar}^n$  and  $U_{i\alpha}^n \neq U_{(i+1/2)al}^n \neq U_{(i-1/2)ar}^n$ . However, for a special reconstruction where  $U_{i\alpha}^n = U_{(i+1/2)al}^n = U_{(i-1/2)ar}^n$ , (3.2) simplifies to

$$g(v) = \sum_{\alpha=1}^2 [\{n_{i\alpha}^n - \lambda v^{+ve} n_{(i+1/2)al}^n + \lambda v^{-ve} n_{(i-1/2)ar}^n\} \delta(v - U_{i\alpha}^n)] + \text{positive terms} \quad (3.3)$$

If  $\lambda$  is chosen such that  $\{n_{i\alpha}^n - \lambda v^{+ve} n_{(i+1/2)al}^n + \lambda v^{-ve} n_{(i-1/2)ar}^n\} > 0$ ,  $g(v)$  will always be non-negative and hence realizability of the corresponding finite-volume scheme can be guaranteed. This marks a significant improvement in the accuracy of solutions using quadrature-based moment methods. Over the years, many high-order finite-volume schemes have been developed [32, 33, 34, 35, 36, 37, 38, 39, 40, 41] for convection dominated problems in the field of fluid dynamics. But the researchers using quadrature-based moment methods have not been benefited by these high-order schemes because of the non-realizability limitation. However, with the new approach, all the already existing information about high-order finite-volume schemes can be utilized for solutions using quadrature-based moment methods.

To summarize, a  $p^{th}$ -order realizable finite-volume scheme uses a  $p^{th}$ -order reconstruction for weights and a 1<sup>st</sup>-order reconstruction for abscissas along with a constraint on  $\lambda$ . The constraint on  $\lambda$ , or the realizability criterion, for any general case is derived in the next section. Before the constraints are derived, certain important things about the new realizable finite-volume scheme must be stated.

Firstly, a  $p^{th}$ -order realizable finite-volume scheme is not exactly  $p^{th}$ -order accurate because of the 1<sup>st</sup>-order reconstruction used for abscissas. The scheme can hence be thought of as a quasi- $p^{th}$ -order scheme. However, said that, it must be stressed that, the abscissas that are used in practical problems are often nearly constant over a range of cells. So even if mathematically speaking, the new scheme may not be  $p^{th}$ -order accurate for more general problems, for most practical problems, it is as good as the  $p^{th}$ -order scheme. This fact is demonstrated in the section on numerical results.

Secondly, the realizability constraint on  $\lambda$  can be applied in two ways. In the first approach,  $\Delta t$  should be computed in each cell satisfying the realizability criterion for quasi- $p^{th}$ -order scheme and then the minimum  $\Delta t$  should be used to advance the solutions. In the second approach,  $\Delta t$  should be computed by satisfying the realizability criterion for the 1<sup>st</sup>-order scheme (2.25). Then a check should be made as to whether that  $\Delta t$  satisfies the realizability criterion for a quasi- $p^{th}$ -order accurate scheme. For the cells in which  $\Delta t$  computed using the realizability criterion of the 1<sup>st</sup>-order scheme does not satisfy the realizability criterion for a quasi- $p^{th}$ -order scheme, 1<sup>st</sup>-order reconstruction for weights instead of  $p^{th}$ -order reconstruction should be used. The later approach is used in the numerical simulations in this paper because it is more suitable for multi-stage time-integration.

### 3.1 Realizability condition for 1D cases

The realizability condition should be satisfied for each quadrature node separately. If in a given cell realizability condition fails for any quadrature node, first order reconstruction should be used for the weight corresponding to that quadrature node. For 1D case with two-node quadrature following two conditions should be satisfied:

$$\begin{aligned} \{n_{i1}^n - \lambda v^{+ve} n_{(i+1/2)1l}^n + \lambda v^{-ve} n_{(i-1/2)1r}^n\} &> 0 \\ \{n_{i2}^n - \lambda v^{+ve} n_{(i+1/2)2l}^n + \lambda v^{-ve} n_{(i-1/2)2r}^n\} &> 0 \end{aligned} \quad (3.4)$$

Replacing  $v^{+ve}$  and  $v^{-ve}$  with  $\max(U_{i1}, 0)$  and  $\min(U_{i1}, 0)$  respectively, (3.4) reduces to

$$\begin{aligned} \{n_{i1}^n - \lambda \max(U_{i1}, 0) n_{(i+1/2)1l}^n + \lambda \min(U_{i1}, 0) n_{(i-1/2)1r}^n\} &> 0 \\ \{n_{i2}^n - \lambda \max(U_{i2}, 0) n_{(i+1/2)2l}^n + \lambda \min(U_{i2}, 0) n_{(i-1/2)2r}^n\} &> 0 \end{aligned} \quad (3.5)$$

### 3.2 Realizability condition for 2D cases

A more general form for (3.5) can be written as:

$$\{n_{i\alpha}^n - \lambda [X(W_{(i+1/2)al}^n, 0) - X(0, W_{(i-1/2)ar}^n)]\} > 0 \quad (3.6a)$$

where definition of  $X$  is similar to  $G$  and is given by

$$X(W_{al}, W_{ar}) = Y^+(W_{al}) + Y^-(W_{ar}) \quad (3.6b)$$

with

$$Y^+(W_{al}) = n_{al} \max(U_{al}, 0) \quad \text{and} \quad Y^-(W_{ar}) = n_{ar} \min(U_{ar}, 0) \quad (3.6c)$$

For 2D cases a more general form of (3.6) can be written as:

$$\left\{ n_{i\alpha}^n - \lambda \sum Flux_{\alpha}^n \right\} > 0 \quad (3.7)$$

where summation is over all the faces of  $i^{th}$  cell. In (3.7), for calculating the fluxes at faces only the reconstructed abscissas on the interior sides (side towards  $i^{th}$  cell) of faces should be used, the ones on the opposite side should be set to zero. In other words, the flux in (3.7), is the outgoing flux for  $i^{th}$  cell and the flux coming in from neighboring cells should not be accounted for.

Consider a simple 2D case, shown in Figure 1. For the sake of simplicity subscript  $\alpha$  and superscript  $n$  will be dropped. Cell 0 has four neighbours – Cell 1, Cell 2, Cell 3, Cell 4 - and the reconstructed values of weights on inner sides of corresponding faces are  $n_{01}$ ,  $n_{02}$ ,  $n_{03}$ ,  $n_{04}$  respectively. The cell averaged weight for  $0^{th}$  cell is  $n_0$  and the corresponding X and Y abscissas are  $U_0$  and  $V_0$  respectively. The realizability condition for this case can be written as:

$$\{n_0 - \lambda[n_{01}A_1 \max(U_0, 0) + n_{02}A_2 \max(V_0, 0) - n_{03}A_3 \min(U_0, 0) - n_{04}A_4 \min(V_0, 0)]\} > 0 \quad (3.8)$$

where  $A_1, A_2, A_3, A_4$  are areas of the four faces. Note for 2D case  $\lambda = \Delta t / vol_i$  where  $vol_i$  is the volume of  $i^{th}$  cell. The same realizability condition can be used for 3D cases as well.

### 3.3 High-order realizable schemes

Here a brief overview of two realizable schemes in 2D and one realizable scheme in 1D is presented. The basic idea is to use high-order reconstruction for weights but piecewise constant reconstruction for abscissas. In fact, the following modifications can be made to step (d) in solution algorithm mentioned above.

d) Reconstruct weights at cell faces using any high-order reconstruction. Use first-order reconstruction for abscissas. Check the realizability condition in cells. For the cells in which realizability condition fails, use first order reconstruction for weights.

With this modification in the solution algorithm, any arbitrarily high-order finite-volume scheme can be used for quadrature-based moment method. This is a significant step, as it makes all the high-order finite-volume schemes developed for fluid flows automatically applicable to quadrature-based moment methods as well. This paper presents results for quasi-2<sup>nd</sup>-order scheme and quasi-3<sup>rd</sup>-order scheme for 1D. For 2D, numerical results using quasi-2<sup>nd</sup>-order scheme is presented.

For 1D cases, both the new schemes - quasi-2<sup>nd</sup>-order and quasi-3<sup>rd</sup>-order – are obtained using MUSCL technique [32, 33, 36, 37]. For quasi-2<sup>nd</sup>-order scheme, a piecewise-linear reconstruction is used for weights while for quasi-3<sup>rd</sup>-order scheme, a piecewise-parabolic reconstruction is used for weights. In both the schemes, a min-mod limiter is used to avoid creation of any new local extrema.

In quasi-2<sup>nd</sup>-order reconstruction for 2D, a least-squares reconstruction [35] is used for weights using the adjacent cell values. Moreover, a Barth limiter [40] is applied to the least-squares reconstruction to avoid spurious oscillations.

## IV. Numerical results

In this section several results are presented for 1D and 2D cases. For all the cases a 2<sup>nd</sup>-order Runge-Kutta scheme has been used for time integration. Periodic boundary conditions have been used for all 1D cases while for the 2D case a combination of wall and fix-all boundary conditions is used. The domain for all 1D cases is defined by  $x \in [-1, 1]$ . All the simulations just consider the spatial flux terms. Collisions and body force terms are not included.

### 4.1 Order of accuracy study

Here order of accuracy of the standard and the new schemes is discussed. Results in this section are based on simple 1D cases for which analytical solutions exist. L1 errors are calculated by comparing the numerical solution with the analytical solution for mean density ( $M^0 = \sum_{\alpha} n_{\alpha}$ ). L1 errors and order of convergence are presented for four schemes – 1<sup>st</sup>-order, standard 2<sup>nd</sup>-order, quasi-2<sup>nd</sup>-order, quasi-3<sup>rd</sup>-order. Table 1 and Table 2 show the results for 1-node quadrature and 2-node quadrature respectively. For 1-node quadrature, initial weight ( $n$ ) and abscissa ( $U$ ) are given as:

$$\begin{aligned} n &= 1.0 + \sin(\pi x) \\ U &= 1.0 \end{aligned} \quad (4.1)$$

For 2-node quadrature, initial weights ( $n_1, n_2$ ) and abscissas ( $U_1, U_2$ ) are given as:

$$\text{for } x < 0: n_1 = |\sin(\pi x)|, n_2 = 0, U_1 = 1, U_2 = 0 \quad (4.2)$$

$$\text{for } x > 0: n_1 = 0, n_2 = |\sin(\pi x)|, U_1 = 0, U_2 = -1$$

It is observed that formal order of accuracy can be obtained for 1-node quadrature but as the number of quadrature nodes is increased, order of accuracy for all the schemes reduces. Although the reason for this loss of order of accuracy has not been studied extensively, it is attributed to the combined effect of an increase in the number of equations and use of moment inversion algorithm for ill-conditioned points. At many points the values of weights are very small and the non-linear equations solved using the moment-inversion algorithm is often ill-conditioned for these points in case of multiple quadrature nodes. It can also be observed that quasi-2<sup>nd</sup>-order scheme always has approximately the same order of convergence as standard 2<sup>nd</sup>-order scheme, and quasi-3<sup>rd</sup>-order scheme is better compared to both.

#### 4.2 Grid convergence study

In this section, grid convergence studies for quasi-2<sup>nd</sup>-order and quasi-3<sup>rd</sup>-order schemes in 1D are presented. For both the schemes, mean density obtained using different grid resolutions is compared with the analytical solution. Four different grids have been considered with the number of cells equal to 25, 50, 100, 200. The comparisons have been done for a 2-node quadrature case with the same initializations as in (4.2). Figure 2(a) and 2(b) show grid convergence for quasi-2<sup>nd</sup>-order and quasi-3<sup>rd</sup>-order schemes respectively. As the number of grid cells is increased, solutions using both the schemes converge towards the analytical solution.

#### 4.3 Comparison of 1D results for a case where abscissas are constant

For this case, 2-node quadrature is used with weights being sinusoidal functions and abscissas being square functions. There are 50 grid points along x axis. The initial (t=0) conditions are shown in Figure 3(a), while Figure 3(b) and 3(c) show the final conditions for mean density and mean velocity respectively (t=1). The weight distribution is symmetric about x=0, with the left wave moving towards the right (-ve abscissa) and the right wave moving towards the left (+ve abscissa). The final time has been chosen such that the waves coalesce at x=0 and then separate again. Four different schemes have been compared - 1<sup>st</sup>-order, standard 2<sup>nd</sup>-order, quasi-2<sup>nd</sup>-order, quasi-3<sup>rd</sup>-order. The standard 2<sup>nd</sup>-order and quasi-2<sup>nd</sup>-order results are on top of each other. As the abscissas are constant over a range of cells, this was inferred in one of the previous sections. Also, the quasi-3<sup>rd</sup>-order scheme shows an improvement over the quasi-2<sup>nd</sup>-order scheme.

#### 4.4 Comparison of 1D results for a case where abscissas are continuously varying

For this case, 4-node quadrature is used with weights being constant and abscissas being sinusoidal functions. The number of grid cells for 1<sup>st</sup>-order scheme is 300. For the standard 2<sup>nd</sup>-order and quasi-2<sup>nd</sup>-order schemes the number of grid cells is 150 while for quasi-3<sup>rd</sup>-order it is 100. The initial (t=0) conditions are shown in Figure 4(a) while Figure 4(b) and 4(c) show final conditions for density and mean velocity respectively (t=1). This case shows the non-realizability problem with standard 2<sup>nd</sup>-order-scheme. The results obtained using standard 2<sup>nd</sup>-order scheme are quite different from the others. Also, the mean density plot for quasi-2<sup>nd</sup>-order scheme is asymmetric about x=0. For the standard 2<sup>nd</sup>-order scheme, realizability of moments is not guaranteed and if the moments go out of realizable space, which is what is happening here, weights and abscissas are not coupled accurately. Although this does not happen all the time, but because realizability is not guaranteed, this can cause wrong computation at any one time step and thereafter the numerical solution strays away from the correct physical solution.

#### 4.5 Comparison of 2D Results

2D results for a dilute impinging-jet problem is presented. The domain consists of a square (7x7) box with two openings on the bottom wall through which jets enter. As the time progresses, the jets cross each others, strike the wall and then rebound. These simulations have been done using 4-node quadrature -  $(n_1, U_1, V_1), (n_2, U_2, V_2), (n_3, U_3, V_3), (n_4, U_4, V_5)$ . The values of weights and abscissas at left opening are:

$$\begin{aligned} n_1 = n_2 = n_3 = n_4 &= 0.1 \\ U_1 = 1.001, U_2 = 0.999, U_3 = 1.0, U_4 &= 1.0 \\ V_1 = 1.001, V_2 = 1.0, V_3 = 0.999, V_4 &= 1.0 \end{aligned} \quad (4.3a)$$

and the values at right opening are:

$$\begin{aligned} n_1 = n_2 = n_3 = n_4 &= 0.1 \\ U_1 = -1.001, U_2 = -0.999, U_3 = -1.0, U_4 &= -1.0 \\ V_1 = 1.001, V_2 = 1.0, V_3 = 0.999, V_4 &= 1.0 \end{aligned} \quad (4.3b)$$

Inside the domain, the weights and abscissas are initialized as:

$$n_1 = n_2 = n_3 = n_4 = 0.001 \quad (4.3c)$$

$$U_1 = -0.001, U_2 = 0.001, U_3 = 0.0, U_4 = 0.0$$

$$V_1 = 0.001, V_2 = 0.0, V_3 = -0.001, V_4 = 0.0$$

Results are presented for 1<sup>st</sup>-order and quasi-2<sup>nd</sup>-order schemes. A computational grid with 2562 triangular cells is used. The solution obtained using 1<sup>st</sup>-order scheme is highly diffusive. The improvement in the solution using quasi-2<sup>nd</sup>-order scheme is clearly evident.

## V. Conclusions

Heretofore, the use of finite-volume schemes in quadrature-based moment methods was limited to 1<sup>st</sup>-order scheme because of the non-realizability problem. But the use of 1<sup>st</sup>-order scheme often leads to highly diffused numerical solutions. Over the years, a huge amount of research has been done for developing high-order finite-volume schemes in the field of Computational Fluid Dynamics. However, the issue of non-realizability, has often acted as a barrier, making the high-order finite-volume schemes inaccessible to those who use models based on quadrature-based moment methods. In the present work, the barrier has been broken by proposing a generalized idea to develop any arbitrarily high-order realizable finite-volume scheme. According to the new idea, a  $p^{th}$ -order realizable finite-volume scheme can be constructed using a  $p^{th}$ -order reconstruction for weights and a 1<sup>st</sup>-order reconstruction for abscissas along with a realizability criterion. Using this approach, a realizable finite-volume scheme of any arbitrary order can be developed. This marks a significant step as it makes all the high-order finite-volume schemes, developed over the years for fluid flows, automatically accessible to researchers using quadrature-based moment methods.

## Acknowledgments

The study was funded by NSF grant CISE-0830214. The views and conclusions herein are those of the authors and should not be interpreted as necessarily representing the official policies or endorsements, either expressed or implied, of NSF or the U.S. Government.

## References

- <sup>1</sup>Desjardins, O., Fox, R. O., and Villedieu, P., "A quadrature-based moment method for dilute fluid-particle flows," *Journal of Computational Physics*, Vol. 227, No. 4, 2008, pp. 2514-2539.
- <sup>2</sup>Fan, R., Marchisio, D. L., and Fox, R. O., "Application of the direct quadrature method of moments to polydisperse gas-solid fluidized beds," *Powder technology*, Vol. 139, No. 1, 2004, pp. 7-20.
- <sup>3</sup>Fede, P., and Simonin, O., "Numerical study of the subgrid fluid turbulence effects on the statistics of heavy colliding particles," *Physics of Fluids*, Vol. 18, No. 4, 2006, pp. 045103-045103-17.
- <sup>4</sup>Fevrier, P., Simonin, O., and Squires, K. D., "Partitioning of particle velocities in gas-solid turbulent flows into a continuous field and a spatially uncorrelated random distribution: theoretical formalism and numerical study," *Journal of Fluid Mechanics*, Vol. 533, 2005, pp. 1-46.
- <sup>5</sup>Fox, R. O., "A quadrature-based third-order moment method for dilute gas-particle flows," *Journal of Computational Physics*, Vol. 227, No. 12, 2008, pp. 6313-6350.
- <sup>6</sup>He, J., and Simonin, O., "Non-equilibrium prediction of the particle phase stress tensor in vertical pneumatic conveying," *Proceedings of the 5<sup>th</sup> International Symposium on Gas-Solid Flows*, Vol. 166, 1993, pp. 253-263.
- <sup>7</sup>Jenkins, J. T., and Savage, S. B., "A theory for the rapid flow of identical, smooth, nearly elastic spherical particles," *Journal of Fluid Mechanics*, Vol. 130, 1983, pp. 187-202.
- <sup>8</sup>Sakiz, M., and Simonin, O., "Numerical experiments and modeling of non-equilibrium effects in dilute granular flows," *Proceedings of the 21<sup>st</sup> International Symposium on Rarefied Gas Dynamics, Cepadues-Editions, Toulouse, France, 1998*.
- <sup>9</sup>Sundaram, S., and Collins, L. R., "Collision statistics in an isotropic particle-laden turbulent suspension. I. Direct numerical simulations," *Journal of Fluid Mechanics*, Vol. 335, 1997, pp. 75-109.
- <sup>10</sup>Passalacqua, A., Fox, R. O., Garg, R., and Subramaniam, S., "A fully coupled quadrature-based moment method for dilute to moderately dilute fluid-particle flows," *Chemical Engineering Science*, 2009, doi:10.1016/j.ces.2009.09.002.
- <sup>11</sup>Passalacqua, A., Galvin, J. E., Vedula, P., Hrenya C. M., and Fox, R. O., "A quadrature-based kinetic model for dilute non-isothermal granular flows," Submitted to *Journal of Fluid Mechanics*
- <sup>12</sup>Fox, R. O., "Optimal moment sets for multivariate direct quadrature method of moments," *Industrial & Engineering Chemical Research*, Vol. 48, No. 21, 2009, pp. 9686-9696.
- <sup>13</sup>Fox, R. O., "Higher-order quadrature-based moment methods for kinetic equations," *Journal of Computational Physics*, Vol. 228, No. 20, 2009, pp. 7771-7791.
- <sup>14</sup>McGraw, R., "Description of aerosol dynamics by the quadrature method of moments," *Aerosol Science And Technology*, Vol. 27, No. 2, 1997, pp. 255-265.
- <sup>15</sup>Benson, D. J., "Volume of fluid interface reconstruction methods for multi-material problems," *Applied Mechanics Reviews*, Vol. 55, 2002, pp. 151-165.

- <sup>16</sup>Gueyffier, D., Li, J., Nadim, A., Scardovelli, R., and Zaleski, S., "Volume-of-fluid interface tracking with smoothed surface stress methods for three-dimensional flows," *Journal of Computational Physics*, Vol. 152, No. 2, 1999, pp. 423-456.
- <sup>17</sup>Rider, W. J., and Kothe, D. B., "Reconstructing volume tracking," *Journal of Computational Physics*, Vol. 141, No. 2, 1998, pp. 112-152.
- <sup>18</sup>Liu, H., Osher, S. and Tsai, R., "Multi-valued solution and level set methods in computational high frequency wave propagation," *Communications in Computational Physics*, Vol. 1, No. 5, 2006, pp. 765-804.
- <sup>19</sup>Osher, S. and Fedkiw, R. P., "Level set methods: An overview and some recent results.," *Journal of Computational Physics*, Vol. 169, No. 2, 2001, pp. 463-502.
- <sup>20</sup>Osher, S. and Sethian, J. A., "Fronts propagating with curvature dependent speed: Algorithms based on Hamilton-Jacobi formulations.," *Journal of Computational Physics*, Vol. 79, No. 1, 1988, pp. 12-49.
- <sup>21</sup>Sethian, J. A. and Smereka, P., "Level set methods for fluid interface," *Annual Review of Fluid Mechanics*, Vol. 35, 2003, pp. 341-372.
- <sup>22</sup>Bird, G. A., *Molecular Gas Dynamics and the Direct Simulation of Gas Flows*, Oxford University Press, 1994.
- <sup>23</sup>Dukowicz, J. K., "A particle-fluid numerical model for liquid sprays," *Journal of Computational Physics*, Vol. 229, No. 2, 1980, pp. 229-253.
- <sup>24</sup>Hadjiconstantinou, N. G., Garcia, A. L., Bazant, M. Z., and He, G., "Statistical error in particle simulations of hydrodynamic phenomena," *Journal of Computational Physics*, Vol. 187, No. 1, 2003, pp. 274-297.
- <sup>25</sup>Fox, R. O., Laurent, F., and Massot, M., "Numerical simulation of spray coalescence in an Eulerian framework: Direct quadrature method of moments and multi-fluid method.," *Journal of Computational Physics*, Vol. 227, No. 6, 2008, pp. 3058-3088.
- <sup>26</sup>Cercigani, C., Illner, R., and Pulvirenti, M., *The Mathematical Theory of Dilute Gases*, Springer-Verlag, 1994.
- <sup>27</sup>Chapman, S., and Cowling, T. G., *The Mathematical Theory of Non-uniform Gases*, 2<sup>nd</sup> ed., Cambridge University Press, 1961.
- <sup>28</sup>Struchtrup, H., *Macroscopic Transport Equations for Rarefied Gas Flows*, Springer, Berlin, 2005.
- <sup>29</sup>Bhatnagar, P. L., Gross, E. P., and Krook, M., "A model for collision processes in gases. I. Small amplitude processes in charged and neutral one-component systems.," *Physical Review*, Vol. 94, No. 3, 1954, pp. 511-525.
- <sup>30</sup>Schiller, L., and Naumann, Z., "A Drag Coefficient Correlation," *Z. Ver. Deutsch. Ing.*, Vol. 77, 1935, pp. 318-320.
- <sup>31</sup>Perthame, B., "Boltzmann type schemes for compressible Euler equations in one and two space dimensions," *SIAM Journal of Numerical Analysis*, Vol. 29, No. 1, 1990, pp. 1-19.
- <sup>32</sup>Knight, D. D., *Elements of Numerical Methods for Compressible Flows*, Cambridge University Press, 2006.
- <sup>33</sup>Van Leer, B., "Towards the ultimate conservative difference schemes V. A second order sequel to Godunov's method," *Journal of Computational Physics*, Vol. 135, No. 2, 1997, pp. 229-248.
- <sup>34</sup>Collela, P., "The piecewise parabolic method for gas-dynamical simulations," *Journal of Computational Physics*, Vol. 54, No. 1, 1984, pp. 174-201.
- <sup>35</sup>Barth, T. J. and Frederickson, P. O., "Higher order solution of the Euler equations on unstructured grids using quadratic reconstruction," *28<sup>th</sup> Aerospace Sciences Meeting, AIAA, Reno, Nevada*, 1990.
- <sup>36</sup>Collela, P., "A direct Eulerian MUSCL scheme for gas dynamics," *SIAM Journal of Scientific and Statistical Computing*, Vol. 6, No. 1, 1985, pp. 104-117.
- <sup>37</sup>Leveque, R., *Finite Volume Methods for Hyperbolic Problems*, Cambridge University Press, 2002.
- <sup>38</sup>Wang, Z. J., "Spectral (finite) volume method for conservation laws on unstructured grids: Basic Formulation," *Journal of Computational Physics*, Vol. 178, No. 1, 2002, pp. 210-251.
- <sup>39</sup>Godunov, S. K., "A finite-difference method for the numerical computation of discontinuous solutions of the equations of fluid dynamics," *Math Sbornik*, Vol. 47, 1959, pp. 271-306.
- <sup>40</sup>Barth, T. J. and Jespersen, D. C., "The design and application of upwind schemes on unstructured meshes," *27<sup>th</sup> Aerospace Sciences Meeting, AIAA, Reno, Nevada*, 1989.
- <sup>41</sup>Wang, Z. J., "High order methods for Euler and Navier Stokes equations on unstructured grids," *Journal of Progress in Aerospace Sciences*, Vol. 43, 2007, pp. 1-47.

**Table 1.  $L_1$  error and order of accuracy of schemes using 1-node quadrature**

Grid Size	$L_1$ error	Order
<i>1<sup>st</sup>-order scheme</i>		
25	0.208472	-
50	0.113948	0.87
100	0.059817	0.93
200	0.030652	0.96
<i>standard 2<sup>nd</sup>-order scheme</i>		
25	0.051274	-
50	0.016097	1.67
100	0.004729	1.77
200	0.001274	1.89

<i>quasi-2<sup>nd</sup>-order scheme</i>		
25	0.051274	-
50	0.016097	1.67
100	0.004729	1.77
200	0.001274	1.89
<i>quasi-3<sup>rd</sup>-order scheme (without limiter)</i>		
15	0.011729	-
25	0.002664	2.90
50	0.000379	2.81
100	0.000066	2.53
<i>quasi-3<sup>rd</sup>-order scheme</i>		
25	0.008800	-
50	0.002060	2.10
100	0.000422	2.29
200	0.000086	2.29

**Table 2.  $L_1$  error and order of accuracy of schemes using 2-node quadrature**

Grid Size	$L_1$ error	Order
<i>1<sup>st</sup>-order scheme</i>		
25	0.210181	-
50	0.148959	0.50
100	0.091377	0.71
200	0.051817	0.82
<i>standard 2<sup>nd</sup>-order scheme</i>		
25	0.075606	-
50	0.029146	1.38
100	0.011892	1.29
200	0.0004583	1.38
<i>quasi-2<sup>nd</sup>-order scheme</i>		
25	0.075606	-
50	0.029146	1.38
100	0.011885	1.29
200	0.004583	1.37
<i>quasi-3<sup>rd</sup>-order scheme</i>		
25	0.023668	-
50	0.009264	1.35
100	0.002929	1.66
200	0.000978	1.58

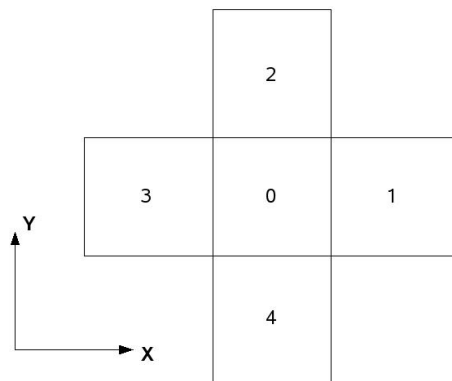
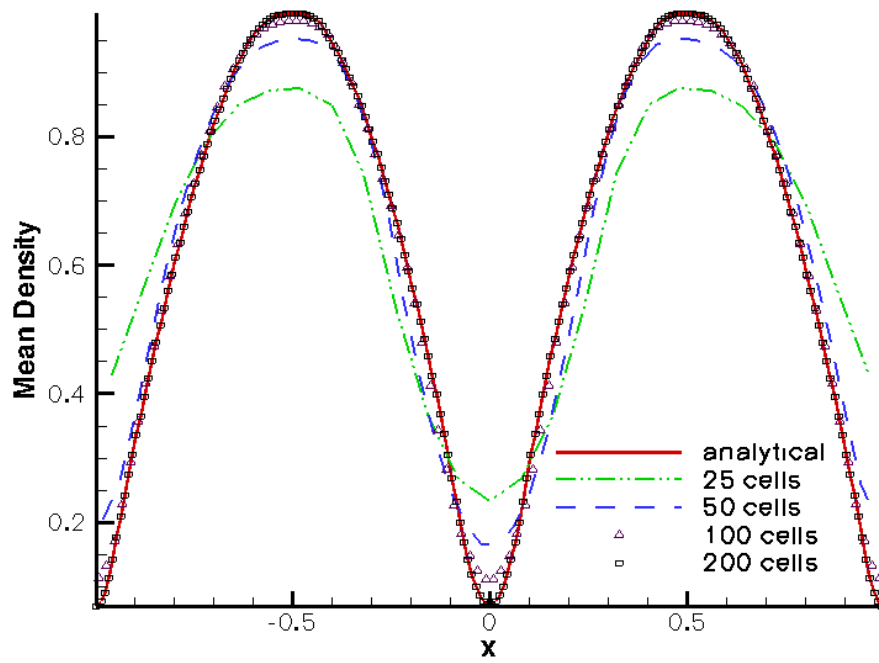
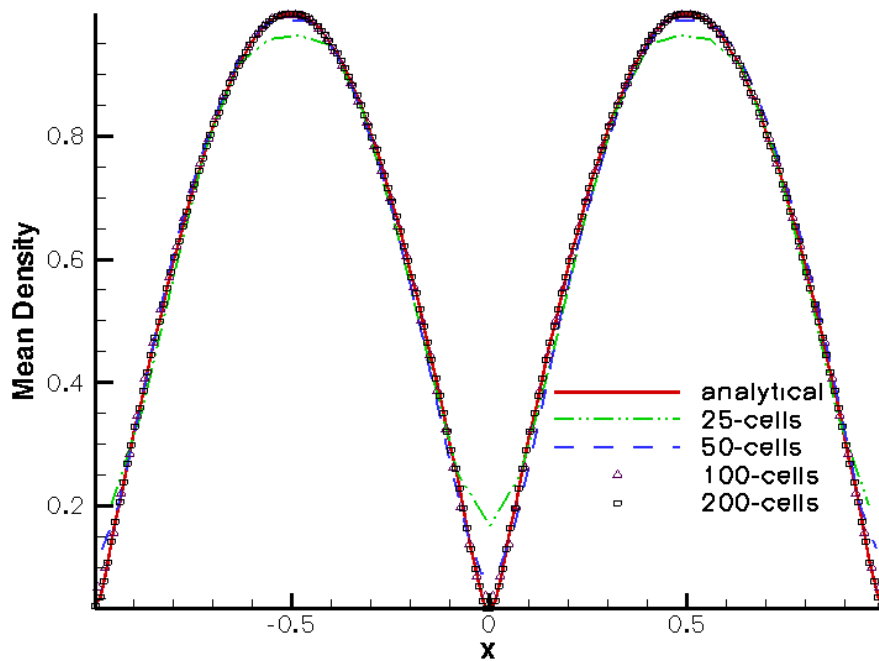


**Figure 1. Cells with faces aligned along Cartesian axes**

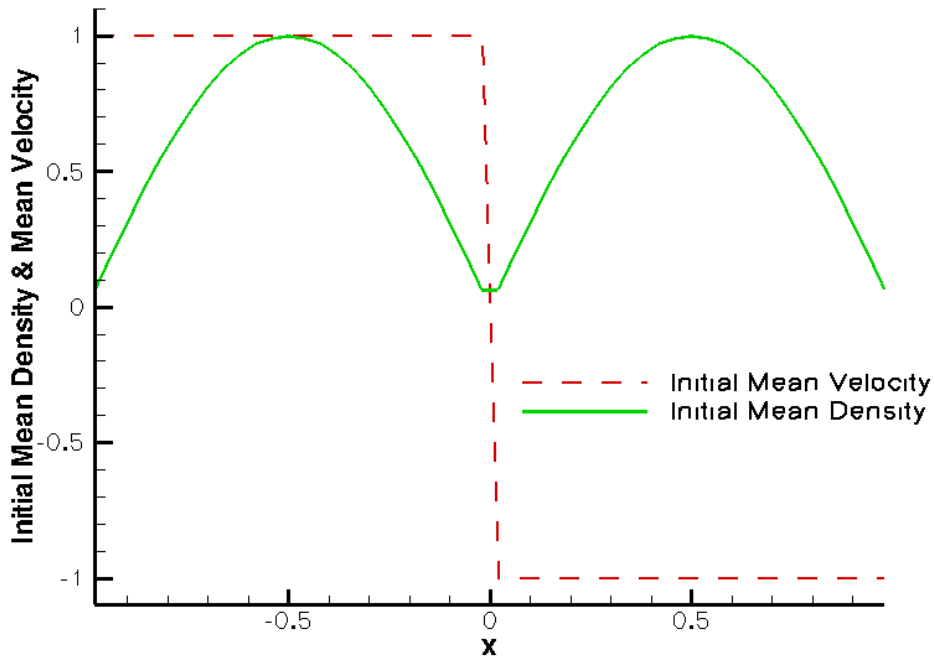


(a) Quasi-2<sup>nd</sup>-order scheme

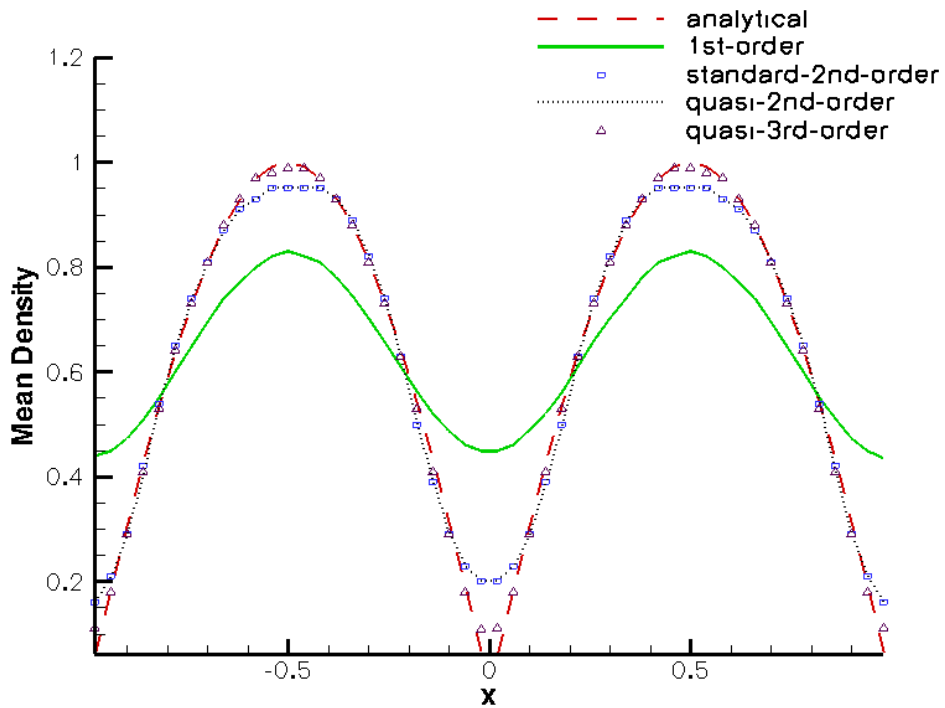


(b) Quasi-3<sup>rd</sup>-order scheme

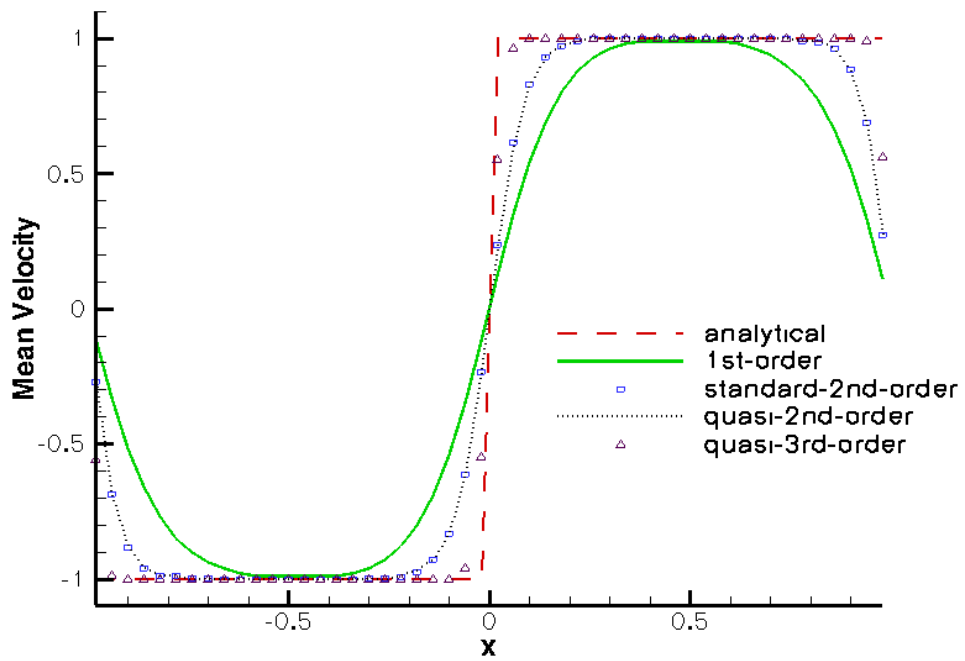
Figure 2. Grid convergence study



(a) Initial mean density and velocity

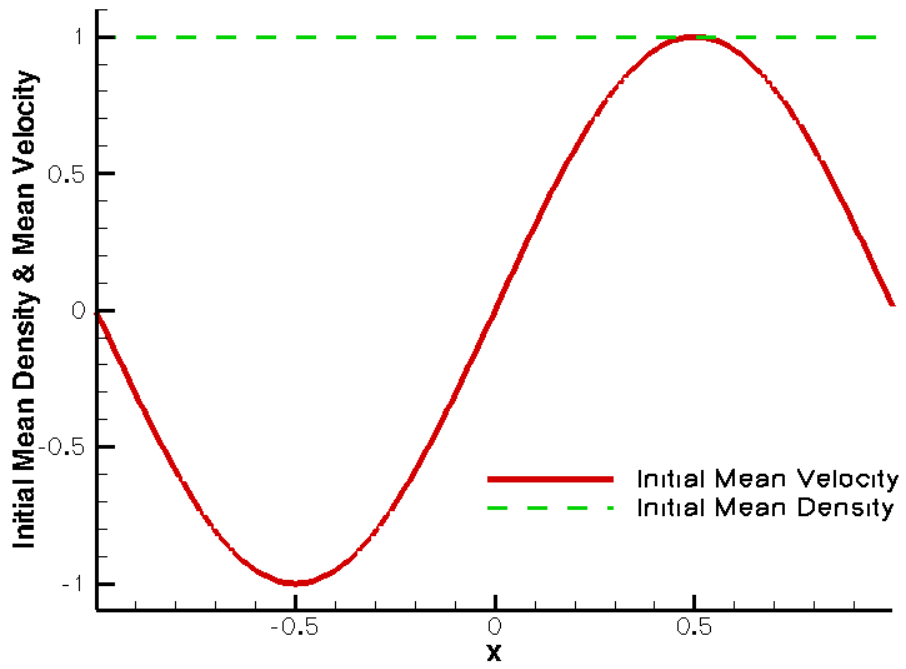


(b) Final mean density

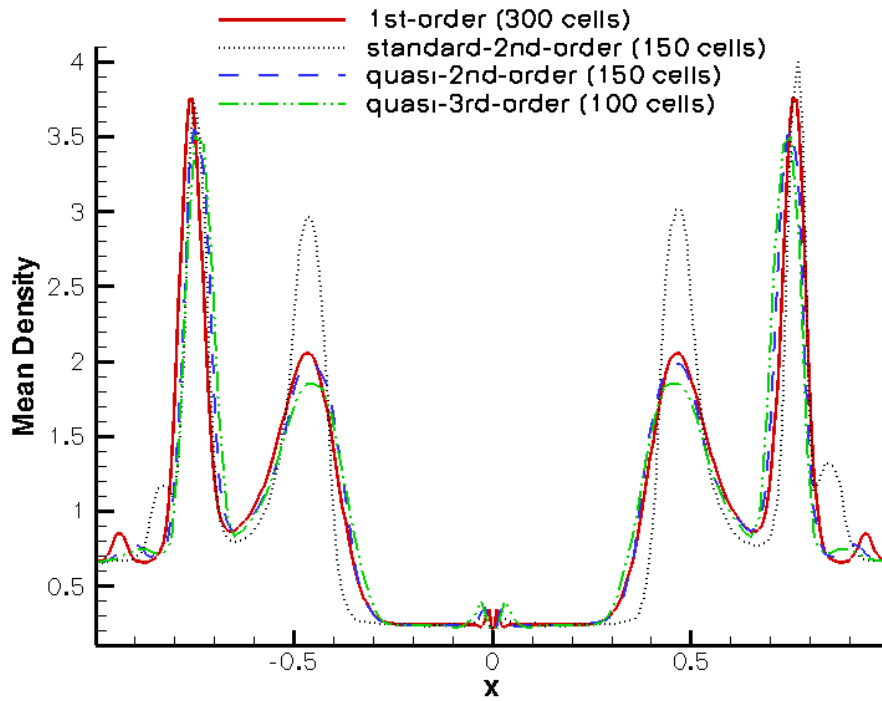


© Final mean velocity

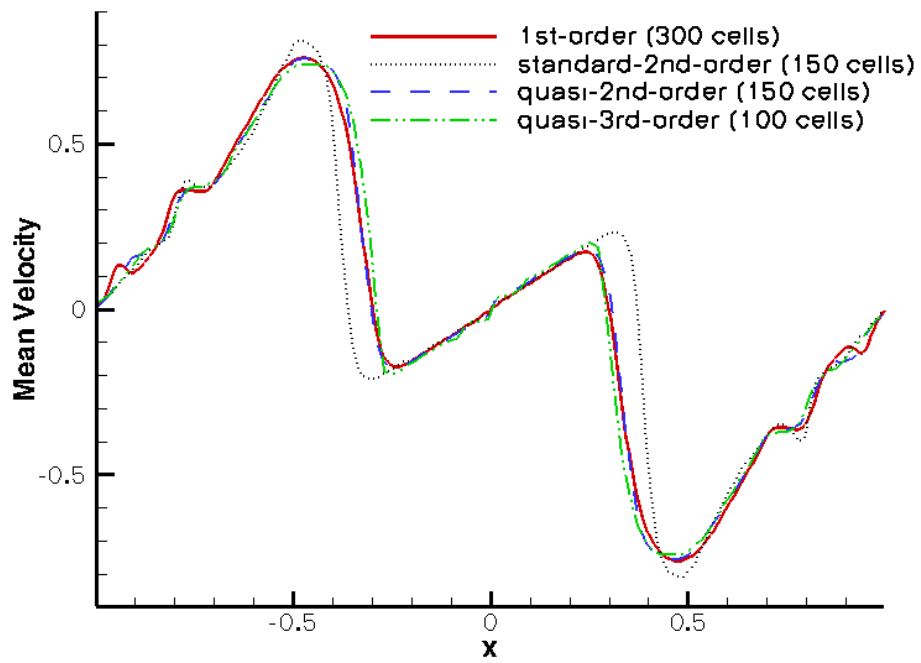
Figure 3. Comparison of schemes for constant abscissa case



(a) Initial mean density and velocity

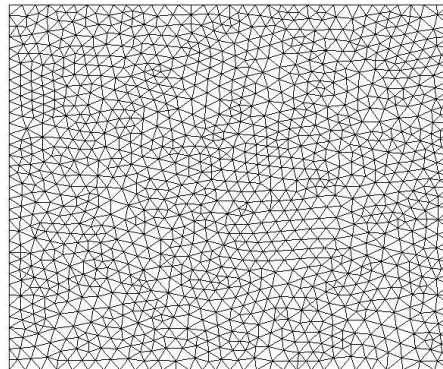


(b) Final mean density

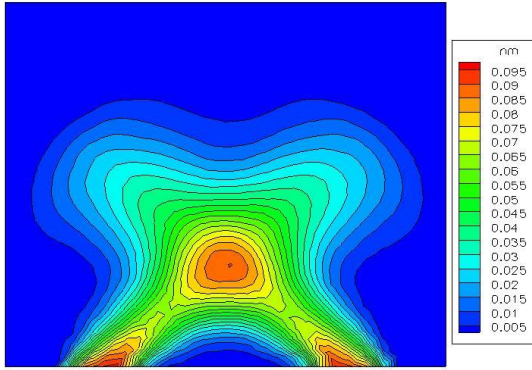


(c) Final mean velocity

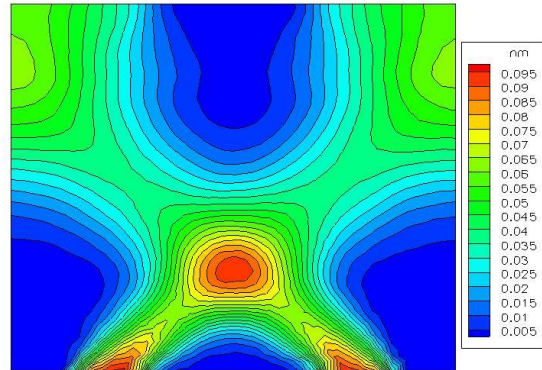
Figure 4. Comparison of schemes for variable abscissa case



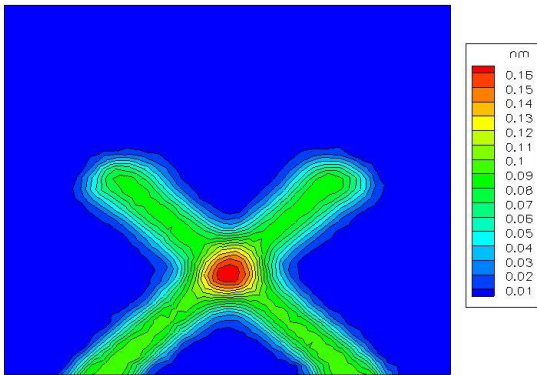
(a) Grid (2562 cells)



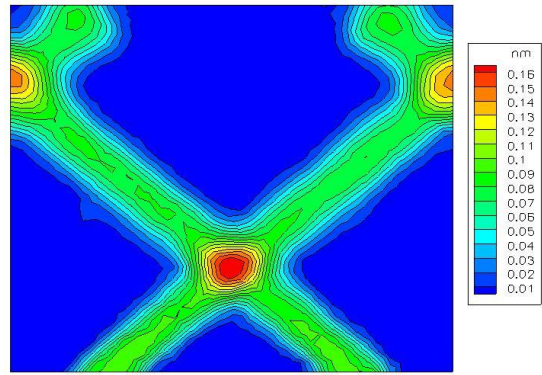
(b) Mean density using 1<sup>st</sup>-order scheme (t = 4)



(c) Mean density using 1<sup>st</sup>-order scheme (t = 7)



(d) Mean density using quasi-2<sup>nd</sup>-order scheme (t = 4)



(e) Mean density using quasi-2<sup>nd</sup>-order scheme (t = 7)

**Figure 5. Dilute impinging jets (2D)**